Research Article Vol. 1, No. 4 / October 2014 / Optica 192

Ultrafast nonequilibrium carrier dynamics in semiconductor laser mode locking

I. Kilen,[1] J. Hader,[2] J. V. Moloney,[1,2,*] and S. W. Koch[3]

[1]Department of Mathematics, Program in Applied Mathematics, University of Arizona, Tucson, Arizona 85721, USA

[2]College of Optical Sciences, University of Arizona, Tucson, Arizona 85721, USA

[3]Department of Physics, University of Marburg, 35032 Marburg, Germany

*Corresponding author: jml@acms.arizona.edu

Received 2 July 2014; revised 15 August 2014; accepted 20 August 2014 (Doc. ID 215263); published 22 September 2014

Semiconductor disk lasers have been shown to be ideal as wavelength-agile, high-brightness sources for producing high average power under various pulsed mode-locking scenarios. Systematic microscopic modeling reveals that ultrafast nonequilibrium kinetic hole burning in electron/hole carrier distributions dictates the outcome of femtosecond duration mode-locked pulse formation. The existence of a large reservoir of unsaturated carriers within the inverted distributions leads to the emergence of multiple pulse waveforms (not necessarily harmonically mode-locked pulse trains) that inefficiently draw on these carrier reservoirs. The concept of gain is no longer meaningful in this limit, and the dynamical inversion of electrons and holes primarily in the active medium establishes the final dynamical state of the system. The simulation results explain much of the generic behavior observed in key recent experiments and point to the difficulty of pushing semiconductor mode-locked lasers to pulse durations below 100 fs.

OCIS codes: (140.3430) Laser theory; (140.7270) Vertical emitting lasers; (140.5960) Semiconductor lasers; (140.7090) Ultrafast lasers.

http://dx.doi.org/10.1364/OPTICA.1.000192

1. INTRODUCTION

Optically pumped vertical external cavity surface emitting lasers (VECSELs) or disk lasers have been shown to be ideal as wavelength-agile, high-brightness sources for numerous applications including CW raw power [1,2], multi-watt single frequency [3], and high average power under various pulsed mode-locking scenarios. Specifically, mode locking has been observed with external semiconductor saturable absorber mirrors (SESAMs) [4–6], integrated quantum well and quantum dot SESAMs [7], and graphene [7,8] and carbon nanotube [9] saturable absorbers. To our knowledge, the shortest fundamental mode-locked pulse duration to date has been 107 fs, albeit at very low average power [10]. While shorter 60 fs pulses have been reported in [11] within longer few picosecond "pulse molecules," we will see that these might also be interpreted as simple interferences between time-shifted, mode-locked picosecond pulses. Rate equation level models using parameters extracted from experiments have proved successful in capturing the mode-locking behavior for longer-duration pulses [12]. As typical intraband carrier scattering times are on the order of 100 fs, it is expected that dynamically changing nonequilibrium distributions will not have a chance to relax to quasi-equilibrium Fermi–Dirac distributions during the pulse itself. The complexity of the nonequilibrium many-body dynamics has limited studies to date to relatively simple ones or multiple quantum-well (QW) single-pass geometries.

In this work, we present a simulation of microscopic many-body effects in the VECSEL gain medium and in the saturable QW absorber by solving the two-band Maxwell Semiconductor Bloch equations (MSBE) in the Hartree–Fock limit using microscopically motivated carrier relaxation and dephasing times. Our simulations show that 100 fs or sub-100 fs pulse mode locking is likely to not be possible in the resonant periodic gain (RPG) active structures under study in this work. Indeed, in Ref. [10], a nonuniform spacing of QWs was used in the low gain limit to broaden the linear net gain to achieve 107 fs pulses. In higher-gain situations, unused carriers can

2334-2536/14/040192-06$15/0$15.00

destabilize the pulse by seeding amplification in spectral windows that exist outside the direct interacting nonequilibrium system. The implications of this are profound and show that it will be extremely difficult to avoid dynamical pulse breakup under strong pump conditions. In particular, we show that the apparent 60 fs pulses observed in [11] are likely due to a pulse splitting into two relatively clean, longer-duration pulses that feed off independent carrier reservoirs in the inverted system. We also identify a clear pulse separation in time at higher pump levels that is consistent with predictions from a very recent record average power mode-locking experiment with a graphene mode-locking element.

2. MICROSCOPIC THEORY AND SIMULATION OF SHORT-CAVITY MODE LOCKING

The theoretical analysis of the VECSEL mode-locking dynamics requires the simulation of the light field $E(z,t)$ propagation inside the laser cavity as well as the nonlinear interaction of this cavity field with the material polarizations $P(z,t)$ of the optically active QW gain region and the QW saturable absorber (SESAM). Assuming that the cavity light field circulates in the z direction, perpendicular to the QW planes, Maxwell's wave equation can be written in the simple form

$$\left[\frac{\partial^2}{\partial z^2} - \frac{n^2}{c_0^2}\frac{\partial^2}{\partial t^2}\right] E(z,t) = \mu_0 \frac{\partial^2}{\partial t^2} P(z,t), \tag{1}$$

where the constants n and c_0 are the background refractive index and the vacuum velocity of light, respectively, and μ_0 denotes the vacuum permeability. The macroscopic polarization $P(z,t)$ is obtained by the summation of the microscopic polarizations $p_{\lambda,\nu,\mathbf{k}}$ over the crystal momentum $\mathbf{k}$ in the plane of the QWs. The dynamics of the microscopic polarization $p_{\lambda,\nu,\mathbf{k}}$ follow from the multiband semiconductor Bloch equations (SBEs) [13]

$$\begin{aligned}\frac{\partial}{\partial t} p_{\lambda,\nu,\mathbf{k}} &= -\frac{i}{\hbar}\sum_{\lambda_1,\nu_1}\left(e^e_{\lambda,\lambda_1,\mathbf{k}}\delta_{\nu,\nu_1} + e^h_{\nu,\nu_1,\mathbf{k}}\delta_{\lambda,\lambda_1}\right)p_{\lambda_1,\nu_1,\mathbf{k}} \\ &\quad - i\left(n^e_{\lambda,\mathbf{k}} + n^h_{\nu,\mathbf{k}} - 1\right)\Omega_{\lambda,\nu,\mathbf{k}} + \Gamma_{\lambda,\nu;\mathrm{deph}}, \\ \frac{\partial}{\partial t} n^{e(h)}_{\lambda(\nu),\mathbf{k}} &= -2\,\mathrm{Im}\left(\Omega_{\lambda,\nu,\mathbf{k}}\left(p_{\lambda,\nu,\mathbf{k}}\right)^{\star}\right) + \Gamma^{e(h)}_{\lambda(\nu);\mathrm{scatt}}.\end{aligned} \tag{2}$$

These equations couple the dynamics of the microscopic polarization $p_{\lambda,\nu,\mathbf{k}}$ and the occupation function $n^{e(h)}_{\lambda(\nu),\mathbf{k}}$, determining the probability that a state $\mathbf{k}$ in the conduction band λ (valence band ν) is occupied by an electron (hole). The renormalized single-particle energies in the Hartree–Fock approximation are

$$\begin{aligned}e^e_{\lambda,\lambda_1,\mathbf{k}} &= \varepsilon^e_{\lambda,\mathbf{k}}\delta_{\lambda,\lambda_1} - \sum_{\lambda_2,\mathbf{q}} V^{\lambda,\lambda_2,\lambda_1,\lambda_2}_{|\mathbf{k}-\mathbf{q}|} n^e_{\lambda_2,\mathbf{q}}, \\ e^h_{\nu,\nu_1,\mathbf{k}} &= \varepsilon^h_{\nu,\mathbf{k}}\delta_{\nu,\nu_1} - \sum_{\nu_2,\mathbf{q}} V^{\nu,\nu_2,\nu_1,\nu_2}_{|\mathbf{k}-\mathbf{q}|} n^h_{\nu_2,\mathbf{q}},\end{aligned} \tag{3}$$

and the renormalized Rabi frequency is

$$\Omega_{\lambda,\nu,\mathbf{k}} = \omega_R + \frac{1}{\hbar}\sum_{\lambda_1,\nu_1,\mathbf{q}\neq\mathbf{k}} V^{\lambda,\nu_1,\nu,\lambda_1}_{|\mathbf{k}-\mathbf{q}|} p_{\lambda_1,\nu_1,\mathbf{q}}. \tag{4}$$

Here, $V(|\mathbf{k}-\mathbf{q}|)$ is the Coulomb potential and $\omega_R = d^{\lambda,\nu}_{\mathbf{k}} E(z,t)/\hbar$, where $d^{\lambda,\nu}_{\mathbf{k}}$ is the dipole-matrix element.

Contributions to the SBE that go beyond the Hartree–Fock approximation describe correlation effects such as dephasing of the polarization (Γ_{deph}), carrier scattering (Γ_{scatt}), and Coulomb screening. In the equation of motion for the carrier distributions [Eq. (2)], the correlation effects in the second Born–Markov approximation lead to Boltzmann-type scattering terms. Inclusion of these terms at this level would make simulation impossible, although we can use the full model with these correlation effects included to assess how quickly a kinetic hole can refill by taking nonequilibrium carrier distributions from the present simulation as initial data.

Together with the wave equation, the SBEs establish the MSBEs. Since the numerical evaluation of the microscopic scattering terms in each time step of a numerical laser dynamics simulation is excessively CPU time demanding, it is often necessary to include the correlation effects on the level of effective rates expressing the net effect of the underlying microscopic processes. In this limit, the dephasing of the polarization is described by a simple decay contribution with the characteristic dephasing time τ_{dep}; $\Gamma_{\lambda,\nu;\mathrm{deph}} = -p_{\lambda,\nu,\mathbf{k}}/\tau_{\mathrm{deph}}$ and, similarly, the carrier-scattering contribution modeling the equilibration of the carrier system follows from $\Gamma_{\lambda(\nu);\mathrm{scatt}} = -(n^{e(h)}_{\lambda(\nu),\mathbf{k}} - f^{e(h)}_{\lambda(\nu),\mathbf{k}})/\tau_{\mathrm{scatt}}$, where $f^{e(h)}_{\lambda(\nu),k}$ is the background quasi-equilibrium distribution of the optically pumped QW and τ_{scatt} governs the characteristic time scales of scattering events. To test our model [14,15] and to study the relevance of nonequilibrium effects, we restrict ourselves to a two-band model, postulating strong confinement of electrons and holes such that only the lowest sub-bands need to be taken into account. In addition, we limit consideration to a parabolic band structure where the transition energy, i.e., the difference between the conduction and valence band energy $\hbar\omega_{\mathbf{k}} = (\hbar^2\mathbf{k}^2/2m_e) + (\hbar^2\mathbf{k}^2/2m_h) + E_g$ is expressible in terms of the effective masses of the electrons m_e, holes m_h, and the bandgap energy E_g. As a sanity check, we employed a full multiband microscopic simulation in a single-pass setting that goes beyond the Hartree–Fock limit to assess the role of ultrafast correlations in the hot carriers (electron/hole) and carrier capture from the pumped barrier to inverted well states. While these can include further pulse-reshaping effects due to kinetic hole filling, we anticipate that the generic features observed in the simple two-band model will be preserved. This will be detailed in a future publication. In the low-gain limit, due to the presence of shallow kinetic holes, these correlations should not significantly affect the results.

We use this model to simulate mode locking in a linear one-dimensional cavity consisting of an AR-coated VECSEL chip consisting of a 10 quantum well RPG active medium and a SESAM at the other end of the cavity. A schematic of the modeled cavity is shown in Fig. 1. We effectively represent tighter focusing on the SESAM by appropriately adjusting the on-axis

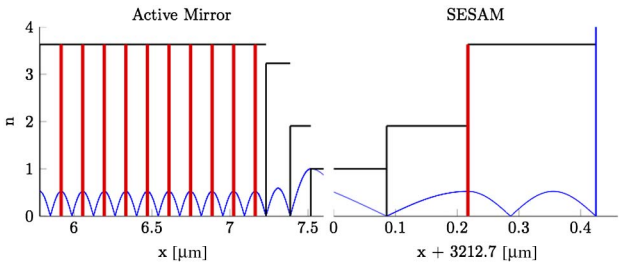

Fig. 1. Schematic of linear cavity with the 10 QW RPG VECSEL chip shown on the left (DBR to the left of this not shown) and a single QW SESAM with spacer and an output coupler. The empty cavity part of the simulation domain in the center is not shown.

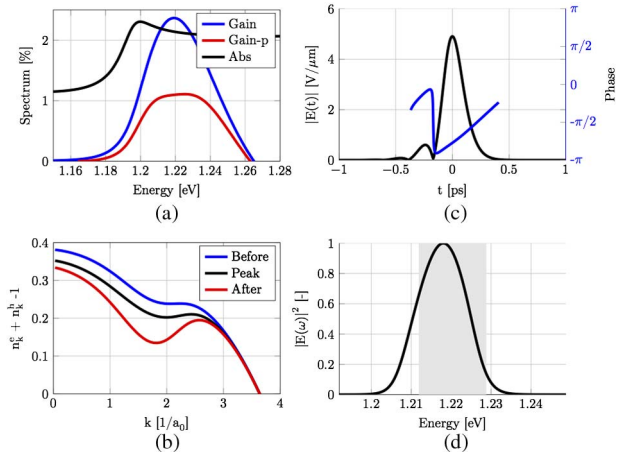

Fig. 2. (a) Plot of the equilibrium gain at a carrier density $n = 1.75 \times 10^{16}$ m^{-2} and at room temperature (blue). Included in this graph is the single QW absorption of the SESAM. The net roundtrip gain is interpreted as the difference of these two curves. (b) Instantaneous snapshots of the inversion in the active VECSEL structure immediately before (blue), at the peak (black), and immediately after the transit of the mode-locked pulse. (c) Plot of the final stable low-power, mode-locked pulse together with the phase across the pulse. (d) Spectrum of the mode-locked pulse. The shaded area shows that this pulse utilizes the full available linear net gain bandwidth.

intensity to represent a ten-fold intensity increase on the SESAM relative to that on the VECSEL chip.

The 10 QW RPG structure modeled here is identical to that employed in Refs. [1,2] to achieve greater than 100 W CW from a VECSEL structure. Details are given therein. We assume a single-layer AR coating on both the VECSEL chip and the SESAM. The VECSEL chip consists of 10 InGaAs QWs grown on an AlGaAs distributed Bragg reflector (DBR), and the SESAM consists of a single InGaAs QW attached to a 1% output coupling mirror. These two components are on opposite sides of a 3.2 cm linear cavity as shown in Fig. 1, with a roundtrip time of approximately 21 ps. We assume a 30 ps (0.5 ps) relaxation time for the QW populations in the VECSEL (SESAM) back to a reference 300 K quasi-equilibrium distribution and the same InGaAs/AlGaAs band structure parameters as for the RPG. The reference distribution density for the SESAM is kept at 5.0e14 [1/m^2], while the density of the QWs in the VECSEL are incremented for the different situations. We stress that the behavior discussed below is expected to be generic in RPG-grown VECSELs.

3. LOW-INVERSION MODE LOCKING

The concept of gain and gain bandwidth is heavily used in discussing and analyzing most mode-locking experiments. For example, a very useful picture that goes back to the seminal early work of Haus [16] utilizes the idea of net gain to estimate the expected characteristic pulse width in a mode-locked setting. This idea works rather well for a host of solid state materials such as fiber lasers, Ti:sapphire, etc. It has also been extensively used to model semiconductor laser mode locking, more recently in a rate equation model of a mode-locked VECSEL [12]. These parameterized models, which may work well for longer pulses, have the built-in assumption that the polarization dynamics is slaved to the driving field and can be adiabatically eliminated. Strictly, this assumption is untrue even for longer picosecond duration pulses, although it appears to work well. However, it is clear from Eq. (2) that the field is driven by the carrier inversion with the latter mediated by the polarization. Because of this, we will focus on the carrier (electron and hole) dynamics in interpreting the results of recent experiments and will only use the term "gain" as a historical reference. Rather than encountering "spectral hole burning," a concept associated with inhomogeneously broadened gain media, we will talk instead about "kinetic hole burning" in the respective carrier distributions.

The situation depicted in Fig. 2 represents a well-behaved dynamical system where the final low average and peak power mode-locked pulse train is stable. The mode-locked pulse has a FWHM of 204 fs and a time–bandwidth product of 0.5. Note the linear chirp across the main pulse and small leading edge subpulse. The pulse substructure is sensitive to the type and degree of dispersion of the single-layer AR coating. In the carrier inversion plots shown in Fig. 2(b), the inversion never bleaches out and simply cycles in a well-controlled fashion between the blue and red curves on each cavity roundtrip. The concept of gain is useful in this limit, as the pulse spectrum shows that the final pulse avails itself of the available linear net gain bandwidth [compare the intersection points of the blue (gain) and black (absorption) curves in Fig. 1(a)]. This low-power, pulsed, mode-locked behavior is akin to that observed in [10].

4. INTERMEDIATE INVERSION PULSE SPLITTING

As the carrier system is driven more strongly by the pump, we observe a fundamental change in the dynamics which cannot be interpreted successfully via a gain model. The key physical quantity of interest is now the inversion $(n^e_{\lambda,\mathbf{k}} + n^h_{\nu,\mathbf{k}} - 1)$ term driving the polarization in Eq. (2), and the dynamics are now unavoidably nonequilibrium. Under strong driving conditions, the initially weak circulating pulse grows and burns a single kinetic hole that recovers after the pulse has left the gain medium. As the pulse becomes stronger and stronger, this transient kinetic hole gets deeper until the inversion is driven

down to zero at pulse center, meaning that there are no carriers available to provide further amplification (gain) in this spectral window. Now, unsaturated carriers in regions spanning both sides of the central spectral window (in the k space) are available to provide amplification, and we observe the emergence of a double-pulse waveform that more effectively utilizes carriers in the inverted medium. In this case, we observe an unusual pulse waveform consisting of two slightly time-shifted, mode-locked pulses whose individual spectra beat to produce an interference or beating that might be misinterpreted as a pulse "molecule" of longer duration (350 fs here), containing a train of shorter (50 fs here) mode-locked pulses. Figure 3 summarizes this behavior in detail.

Figure 3(a) depicts the unsaturated (linear) gain and saturable absorber (SESAM) loss; the net linear gain of the system can be read off from this figure. In comparison to the single-pulse mode-locking scenario of Fig. 2, the dynamical behavior of the inversion now shows two kinetic holes, i.e., two minima in the carrier inversion. This results from the fact that the circulating pulse has evolved to a self-reproducing dynamical state that efficiently extracts carriers from two spectrally separate reservoirs. The interference between these two temporally split pulses could be misinterpreted as individual 50 fs mode-locked pulses within a ps duration "pulse molecule." We observe that this interference effect is rather robust at intermediate pump levels. Finally, inspection of the two separate spectral peaks in Fig. 3(b) shows that, while the full spectral gain bandwidth is spanned when compared to Fig. 3(a), now a large chunk in the middle is not utilized.

Instead, two well-separated spectral peaks emerge, with each associated with independent time-separated pulses. We note

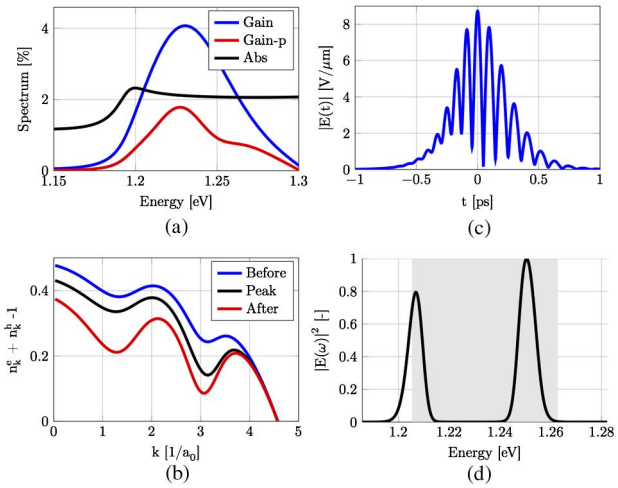

Fig. 3. (a) Similar plot to Fig. 1(a) except that the carriers are now driven more strongly by the pump with density $n = 2.4 \times 10^{16}$ m^{-2} and at room temperature. The net gain is again the difference between the blue (gain) and black (SESAM QW absorption). (b) The electron momentum resolved (k) inversion now shows a double depression and again cycles back and forth between the blue and black curve every roundtrip. (c) Mode-locked pulse waveform showing a beating between two slightly shifted sub-ps-duration pulses. (d) Split spectral peaks, each associated with slighted time-shifted single pulses.

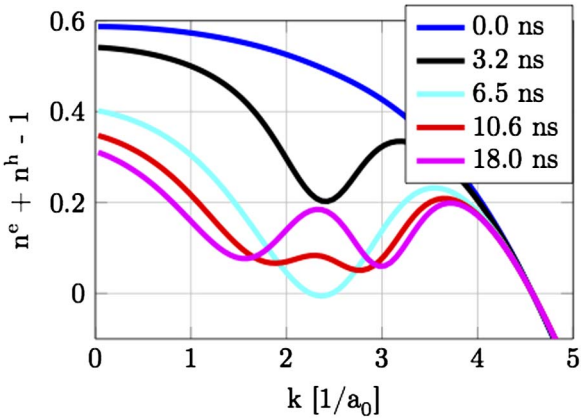

Fig. 4. Development of dual kinetic holes in the inversion starting from an initial Fermi distribution at $t = 0$. The inversion goes negative transiently prior to splitting into two kinetic holes.

here that we can indeed verify (not shown) that this modulated pulse waveform can be spectrally filtered and identified with individual approximate duration 235 fs pulses.

The inversion depicted in Fig. 3 captures an asymptotic, long-time dynamical state of the mode-locked cavity where the pulse has stabilized. However, the dynamical evolution to this final state is somewhat involved and the usual net gain interpretation has to be supplanted by a fully nonequilibrium, kinetic hole-burning one. Prior to the development of the dual split kinetic holes depicted in Fig. 3, we observe a dynamical transient growth of the pulse waveform to the point where the inversion in the vicinity of the central frequency is fully bleached and the subsequent evolution avails itself of unsaturated carrier reservoirs to the high- and low-frequency side of this central frequency. This picture is shown in Fig. 4.

5. HIGH-INVERSION PULSE SPLITTING

At even higher pump levels, there can be too much unsaturated gain for the absorber to clean up. This will drive the generation of new pulses in the cavity that can result in pulse trains, harmonically mode-locked pulses, etc. A special case is when one has the correct amount of absorption (and/or the faster recovery time); it is then possible to obtain a situation in which the time-separated pulses from Section 4 split into two time-shifted pulses. This splitting is simply a further manifestation of the interference observed in Section 4, but now the individual pulses become trapped in their own local potentials and essentially behave as independent mode-locked entities.

This behavior bears a close resemblance to a very recent experimental result that demonstrated up to 10 W of average power in a graphene mode-locked VECSEL. In this work it is argued, based on an observed two-peaked pulse spectrum for average powers exceeding 6 W, that pulse splitting into two temporally separated stable pulses with locally flat phases is the likely interpretation of the experimental data. This would mean that the 10 W average power would be shared between both pulses, say approximately 5 W in each pulse.

Figure 5 summarizes the mode-locked behavior at these higher carrier densities (pump levels). The main difference here

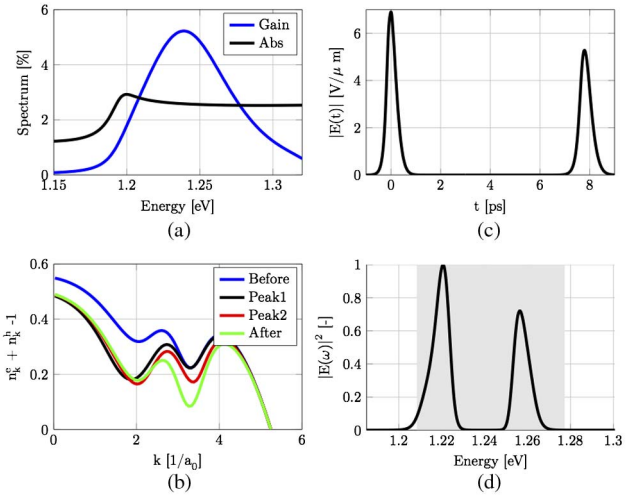

Fig. 5. (a) Linear gain and SESAM absorption spectrum at higher pump levels. (b) Strongly distorted nonequilibrium carrier inversions now show four curves, with the two intermediate ones at the peak of each time-separated pulse. (c) Time-separated, mode-locked pulses and (d) spectrum of both pulses.

is that both pulses no longer overlap but are well separated in time and spectrally. The nonequilibrium inversion has again bleached out in the center, causing two independent pulses to draw from separate carrier reservoirs. In our model, these behaviors are robust over a range of initial carrier densities. Again, by spectral filtering, we can show that each individual pulse is identified with a single peak in the above spectrum.

6. ROLE OF SATURABLE ABSORBER RELAXATION IN CLEANING UP PULSES

We now discuss the influence of the SESAM fast saturable decay rate on the mode-locked pulse behavior observed in the last two sections. If the absorber relaxes sufficiently fast (~500 fs), it can act to damp out any residual amplification resulting from

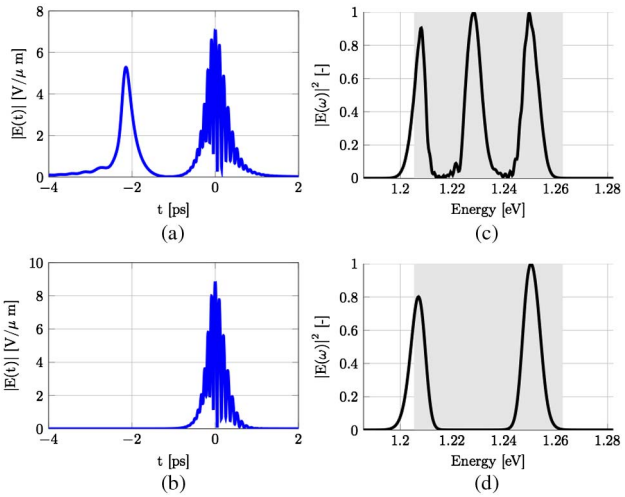

Fig. 6. (a) Emergence of mode-locked pulse train with a slow saturable absorber. (b) Cleaned up single pulse with fast saturable absorber. (c) Triple-peaked spectrum of mode-locked pulses. (d) Double-peaked spectrum of interfering mode-locked pulses (see Fig. 3).

unsaturated carriers in the active structure and consequently clean up the mode-locked pulse train. We illustrate this behavior for the case of the emergence of multiple pulses for a slow saturable absorber in Fig. 6. The triple-pulse waveform (two interfering as in Fig. 3) shown in Fig. 6 and its associated triple peak spectrum can be cleaned up if the saturable absorber relaxes fast enough to prevent the growth of the secondary pulses. We observe a clean mode-locked double pulse with a double spectral peak if we employ the faster saturable absorber in the cavity.

7. RESULTS AND CONCLUSIONS

Our microscopic simulations show that nonequilibrium carrier distributions within inverted QWs in a RPG VECSEL structure are so strongly modified under strong pumping conditions that the nonequilibrium gain saturation picture becomes irrelevant. Our results show that it will be challenging to generate high peak and average power mode-locked pulses from these semiconductor disk lasers. The underlying physics here is fundamentally different from that encountered in other solid state gain media (Ti:sapphire, Er-doped fiber, etc.) or in QD mode-locked VECSELs, as the carriers are free to move in the in-plane dimension. Here, when the carriers contributing to direct amplification are bleached out, the system self-adapts to form uncoupled carrier reservoirs that sustain independent multiple pulses in the cavity.

Our results show that, when bleached out at high pump levels, nonequilibrium carrier distributions dynamically adjust so as to promote independent carrier reservoirs that feed separate pulses within the cavity. These can, for example, create the illusion that a "pulse molecule" is formed, containing even shorter mode-locked pulse trains at certain pump levels. While this work isolates uniquely nonlinear nonequilibrium features that profoundly modify the nature of ultrafast mode locking in semiconductor disk lasers, we expect that these observations will apply to edge emitting structures. However, the latter will be further complicated by long gain paths in contrast to the very thin gain regime in the disk geometry.

Finally, we need to point out that there are many other players involved in influencing the final pulse waveforms. In this work, we have restricted our study to a two-band model and a fixed single-layer AR coating with its own intrinsic dispersion. It is clear that coatings designed for narrow-band CW lasers will exhibit strong dispersion away from the designed wavelength. The net dispersion in the cavity will involve contributions from the transient nonlinear field-induced refractive index in addition to from linear dispersive elements such as DBRs, AR coatings, and mirrors. It is anticipated that these contributions can likewise be optimized to reduce nonlinear chirp and produce ultrashort bandwidth-limited pulses.

FUNDING INFORMATION

Air Force Office of Scientific Research (AFOSR) (FA9550-14-1-0062).

REFERENCES

1. B. Heinen, T.-L. Wang, M. Sparenberg, A. Weber, B. Kunert, J. Hader, S. W. Koch, J. V. Moloney, M. Koch, and W. Stolz,

"106 W continuous-wave output power from vertical-external-cavity surface-emitting laser," Electron. Lett. **48**, 516 (2012).
2. T.-L. Wang, B. Heinen, J. Hader, C. Dineen, M. Sparenberg, A. Weber, B. Kunert, S. W. Koch, J. V. Moloney, M. Koch, and W. Stolz, "Quantum design strategy pushes high-power vertical external cavity surface emitting lasers beyond 100 W," Laser Photon. Rev. **6**, L12–L14 (2012).
3. A. Laurain, C. Mart, J. Hader, J. V. Moloney, B. Kunert, and W. Stolz, "15 W single frequency optically pumped semiconductor laser with sub-MHz linewidth," IEEE Photon. Technol. Lett. **26**, 131–133 (2014).
4. M. Scheller, T.-L. Wang, B. Kunert, W. Stolz, S. W. Koch, and J. V. Moloney, "Passively mode-locked VECSEL emitting 682 fs pulses with 5.1 W of average output power," Electron. Lett. **48**, 588–589 (2012).
5. K. G. Wilcox, A. C. Tropper, H. E. Beere, D. A. Ritchie, B. Kunert, B. Heinen, and W. Stolz, "4.35 kW peak power femtosecond pulse mode-locked VECSEL for supercontinuum generation," Opt. Express **21**, 1599–1605 (2013).
6. M. Hoffmann, O. D. Sieber, V. J. Wittwer, I. L. Krestnikov, D. A. Livshits, Y. Barbarin, T. Südmeyer, and U. Keller, "Femtosecond high-power quantum dot vertical external cavity surface emitting laser," Opt. Express **19**, 8108–8116 (2011).
7. C. A. Zaugg, Z. Sun, V. J. Wittwer, D. Popa, S. Milana, T. S. Kulmala, R. S. Sundaram, M. Mangold, O. D. Sieber, M. Golling, Y. Lee, J. H. Ahn, A. C. Ferrari, and U. Keller, "Ultrafast and widely tuneable vertical-external-cavity surface-emitting laser, mode-locked by a graphene-integrated distributed Bragg reflector," Opt. Express **21**, 31548–31559 (2013).
8. S. Husaini and R. A. Bedford, "Antiresonant graphene saturable absorber mirror for mode-locking VECSELs," (private communication, 2013).
9. K. Seger, N. Meiser, S. Y. Choi, B. H. Jung, D.-I. Yeom, F. Rotermund, O. Okhotnikov, F. Laurell, and V. Pasiskevicius, "Carbon nanotube mode-locked optically-pumped semiconductor disk laser," Opt. Express **21**, 17806–17813 (2013).
10. P. Klopp, U. Griebner, M. Zorn, and M. Weyers, "Pulse repetition rate of 92 GHz or pulse duration shorter than 110 fs from a mode-locked semiconductor disk laser," Appl. Phys. Lett. **98**, 071103 (2011).
11. A. H. Quarterman, K. G. Wilcox, V. Apostolopoulos, Z. Mihoubi, S. P. Elsmere, I. Farrer, D. A. Ritchie, and A. Tropper, "A passively mode-locked external-cavity semiconductor laser emitting 60-fs pulses," Nat. Photonics **3**, 729–731 (2009).
12. O. D. Sieber, M. Hoffmann, V. J. Wittwer, M. Mangold, M. Golling, B. W. Tilma, T. Südmeyer, and U. Keller, "Experimentally verified pulse formation model for high-power femtosecond VECSELs," Appl. Phys. B **113**, 133–145 (2013).
13. H. Haug and S. W. Koch, *Quantum Theory of the Optical and Electronic Properties of Semiconductors* (World Scientific, 2009).
14. A. Baumner, S. W. Koch, and J. V. Moloney, "Non-equilibrium analysis of the two-color operation in semiconductor quantum-well lasers," Phys. Status Solidi B **248**, 843–846 (2011).
15. J. V. Moloney, I. Kilen, A. Bäumner, M. Scheller, and S. W. Koch, "Nonequilibrium and thermal effects in mode-locked VECSELs," Opt. Express **22**, 6422–6427 (2014).
16. H. A. Haus, "Mode-locking of lasers," IEEE J. Sel. Top. Quantum Electron. **6**, 1173–1185 (2000).